Pergamon

Int. J. Multiphase Flow Vol. 22, No. 2, pp. 307–324, 1996

0301-9322(95)00069-0
0301-9322/96 $15.00 + 0.00

THEORETICAL INVESTIGATION OF THE DIAMETER EFFECT ON FLOODING IN COUNTERCURRENT FLOW

S. JAYANTI[1], A. TOKARZ[2] and G. F. HEWITT[3]†

[1]Indian Institute of Technology, Madras, India

[2]Universität Hannover, Hannover, Germany

[3]Department of Chemical Engineering, Imperial College, London SW7 2BY, U.K.

(*Received 18 July 1994; in revised form 6 September 1995*)

Abstract—Calculations have been performed using the CFDS-FLOW3D computational fluid dynamics code to determine the force exerted on a standing wave by gas flowing over it. It is found that the drag on the wave is mainly due to the pressure variation around it and that it is a strong function of the channel dimensions. Extension of these results to typical flooding conditions in countercurrent flow in vertical tubes shows that the gas velocity required to transport waves upwards increases significantly as the tube diameter increases. It is suggested therefore that the mechanism of flooding depends on the diameter of the tube and that flooding is induced by upward transport of waves from near the bottom of the tube in small diameter tubes whereas in large diameter tubes, it may occur due to entrainment and carryover of droplets near the liquid entry.

Key Words—Gas–liquid flow, flooding, waves, interfaces, annular flow.

1. INTRODUCTION

Countercurrent flow of gas and liquid in vertical tubes, channels, tube bundles and packed beds is encountered in a wide variety of chemical, process and nuclear power industries. The flow consists of a liquid film flowing down the wall of a channel with the gas or vapour phase flowing upwards in the countercurrent flow direction. For moderate liquid and gas velocities, the two phases interact little with each other. However, as the gas velocity increases, the interaction becomes stronger and at sufficiently high gas velocities, the countercurrent flow breaks down, i.e. the liquid phase is carried upwards either partly or fully with the gas phase. The onset of this breakdown is called *flooding*; here, part of the liquid flows down while the rest flows upwards with the gas. At higher gas velocities, all the liquid is carried upwards. If the gas velocity is now reduced, there will be a gas velocity at which the liquid flow direction reverses and part of the liquid begins to flow down. The condition at which this occurs is known as *flow reversal*. Flooding and flow reversal constitute the major limiting factors in processes such as mass transfer in packed columns, reflux condensation and nuclear reactor cooling systems.

Although the flooding phenomenon has been the subject of extensive research over a number of decades, controversy still exists as to the exact mechanism of flooding. There are two widely accepted mechanisms of flooding: (A) the formation and upward transport of a large wave from the bottom of the countercurrent flow column, and (B) the occurrence of an instability at the liquid feed inlet resulting in the formation of large waves, part of which are entrained and redeposited in the form of droplets beyond the point of liquid entry. The first of these is supported by extensive experimental evidence (Hewitt & Wallis 1963; Hewitt *et al.* 1965; Shearer & Davidson 1965; McQuillan *et al.* 1985; Govan *et al.* 1991). It was observed in these and other experiments that the waves travelling downwards on the liquid film increased in size the further down they went. Also the wave amplitude increased sharply as the gas velocity approached the flooding point. It was therefore proposed that flooding occurred when a large wave, formed on the liquid film near the liquid exit, could be swept upwards beyond the liquid entry by the force exerted by the gas. Such waves were observed under flooding conditions by many researchers, for example by Hewitt

†Author for correspondence.

et al. (1965), Suzuki & Ueda (1977), McQuillan *et al.* (1985) and Govan (1990). For sufficiently small tube diameters, bridging of the tubes by the growing waves has also been reported (Feind 1960; Imura *et al.* 1977).

In contrast to the above, the second mechanism, which is also supported by experimental evidence (Dukler & Smith 1979; Zabaras & Dukler 1988; Biage *et al.* 1989), attributes flooding to events happening near the liquid inlet. It was found in these experiments that the effect of increasing gas velocity was to create large amplitude waves closer to the liquid inlet. Flooding occurred when the gas velocity was such that large waves occurred at or very close to the point of liquid entry. Under these conditions, droplets would be ripped off the crests of these waves and would be carried further upwards by the gas stream. No upward moving waves were detected in the experiments. Biage (1989) reported however that close to the flooding gas velocity, some large waves started to move upwards, but then slowed down immediately and then fell downwards again.

There is thus contradictory evidence as to the mechanism of flooding. Some of the uncertainty is due to the inlet and outlet conditions which are known to have a strong effect on the flooding velocities (Bankoff & Lee 1986; Govan *et al.* 1991). Govan *et al.* reproduced the form of entrance used by Dukler & Smith (1979) and Zabaras & Dukler (1988) and showed that, with this type of entrance, flooding was initiated at much lower velocities than with the porous wall liquid injection and removal system used by Hewitt & Wallis (1963), Hewitt *et al.* (1965), McQuillan *et al.* (1985) and Govan *et al.* (1991) themselves in a second set of experiments. An important feature of this arrangement is that it allows the gas velocity profile to be fully developed in the tube upstream of the liquid exit and there are no effects associated with vena contracta in the gas phase near the liquid exit zone. This suggested that the droplet entrainment mechanism would only manifest itself for small diameter tubes when flooding was prematurely initiated by the use of end conditions in which the liquid outlet and the gas inlet were such as to lead to wave formation at lower flow rates. In these circumstances, large waves could form near the liquid exit but the gas velocity would not be high enough to transport them upwards. However, droplet entrainment from these waves would still be possible and these droplets could be transported by the gas to region above the liquid inlet, manifesting a form of the flooding phenomenon. Thus, the experiments of Govan *et al.* (1991) provide a coherent explanantion for the apparent inconsistencies in the literature on this subject.

However, the experiments of Biage *et al.* (1989) are in apparent contradiction of the synthesis by Govan *et al.* (1991). Biage *et al.* used porous wall inlet and outlet sections and observed that flooding occurred without wave transport and and that it appeared to result in droplet entrainment. Thus, even if the confusion from badly controlled inlet conditions is removed, the Biage *et al.* results show that the wave growth and transport mechanism cannot be said to be universally prevalent.

A similar contradiction exists in the correlations for flooding. There are two types of well-established correlations for flooding, viz. those of the Wallis type and those of the Kutateladze type:

$$\sqrt{U_G^*} + C_1\sqrt{U_L^*} = C_2 \quad \text{(Wallis type)} \qquad [1]$$

where

$$U_G^* = U_G\sqrt{\frac{\rho_G}{gD\Delta\rho}}$$

and

$$U_L^* = U_L\sqrt{\frac{\rho_L}{gD\Delta\rho}}$$

$$\sqrt{Ku_G^*} + C_3\sqrt{Ku_L^*} = C_4 \quad \text{(Kutateladze type)} \qquad [2]$$

where

$$Ku_G^* = U_G\left(\frac{\rho_G^2}{g\sigma\Delta\rho}\right)^{1/4}$$

and

$$Ku_L^* = U_L\left(\frac{\rho_L^2}{g\sigma\Delta\rho}\right)^{1/4}$$

Here, U_G and U_L are the superficial velocities of the gas and the liquid phases, ρ_G and ρ_L are their respective densities, $\Delta\rho$ the density difference between the phases, σ the surface tension, g the acceleration due to gravity, D the tube diameter and C_1–C_4 are constants which depend to some extent on other parameters such as inlet/outlet conditions and the tube length. Equation [1] is widely used for correlating flooding data in tubes (Wallis 1961; Hewitt & Wallis 1963; Clift *et al.* 1966; Dukler & Smith 1979) while equation [2] has been used to correlate data in tube bundles (Sun 1979; Bradford & Simpson 1987; Kokkonen & Tuimisto 1990).

The interesting difference between these two correlations is that while the Wallis-type correlation (equation [1]) involves the tube diameter, the Kutateladze type (equation 2) does not. For typical values of the U_L^*, the flooding gas velocities predicted by the two correlations agree closely for a tube diameter of 50 mm, and diverge on either side. This is shown in figure 1, where the predictions of equation [1] with C_1 and C_2 equal to 1 and 0.88, respectively, (correlation of Hewitt & Wallis 1963) are compared with those of equation [2] with C_3 and C_4 equal to 1 and 1.79, respectively, (correlation of Sun 1979). For $D = 50$ mm, there is good agreement between the two, while the predictions of equation [2] are higher than those of equation [1] for $D < 50$ mm and lower for $D > 50$ mm.

We propose in the present paper that the two contradictions are related and that the tube diameter (or the geometry of the cross-section) plays an important role in determining which of the two mechanisms/correlations of flooding prevails. The reason for this is as follows. For mechanism A (wave transport) to occur, the gas force on the waves should be large. This can only happen in small diameter tubes where a circumferentially coherent, ring-type wave could be formed. The gas would then be forced to flow over this wave, and there would be a high form drag on the wave. In small tubes, a large wave causes a relatively large reduction in the flow area available for gas at the wave crest, which would increase the form drag on the wave. As a result, the whole

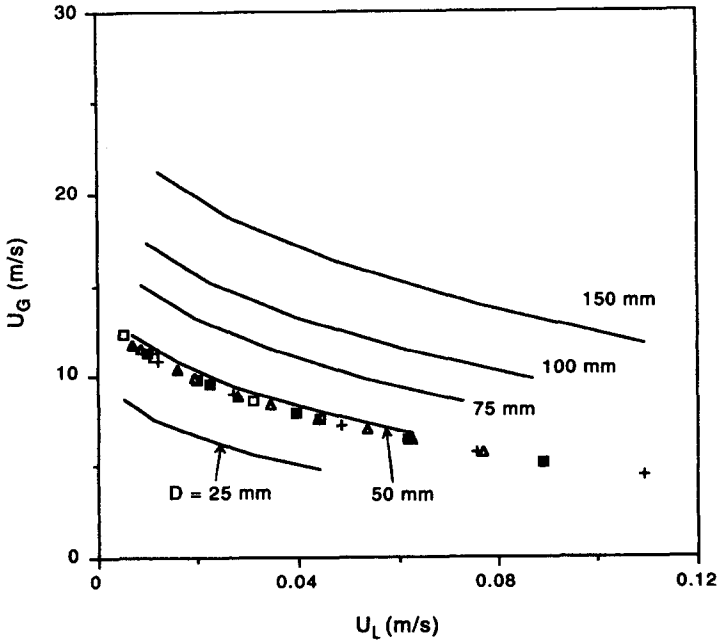

Figure 1. Comparison of the gas velocity required for flooding predicted by the Wallis type of correlation (lines) with that predicted by the Kutateladze type of correlation (squares etc.) for typical liquid velocities and for various tube diameters. The figure shows that the two correlations agree for a tube diameter of 50 mm.

wave could be swept upwards. In large diameter tubes, a circumferentially coherent wave could not easily be formed, and any waves would cover only part of the circumference at any axial position. All the gas is therefore not forced to go over the wave. Also, the reduction in the flow area at the wave crest is relatively less. Both these would mean that the form drag on the wave would be less in a large diameter tube and that a high gas velocity may be required to move the wave upwards. Even if a circumferentially coherent wave was formed, it would be unstable and could not be transported, as a whole, over long distances. For example, Biage *et al.* (1989) observed in his experiments in a 250 × 25 mm channel that some large waves started to move upwards but fell back immediately. Note that although the channel height was only 25 mm, a coherent wave could not be formed in this case because of the large width (250 mm) of the channel. Thus, it would be relatively more difficult for mechanism A to prevail in tubes with large linear dimensions or diameter. In such tubes, large amplitude waves formed over part of the circumference would be a source of droplets which are usually torn off the crests of the waves. Flooding would occur when these large amplitude waves were formed close to the point of liquid entry so that the entrained droplets could be carried off beyond the liquid injection point. This is mechanism B.

Such a scenario is also consistent with the prevalence of the Wallis and the Kutateladze types of correlations for experimental data. The data for the former correlation comes mainly from tubes of $D < 50$ mm in which it is relatively easier for mechanism A to occur. The Kutateladze correlation has been used mainly for flow outside tubes (arranged in bundles). In this case, it is unlikely that a coherent wave will be formed on all adjacent tubes at the same time, and mechanism A may therefore be suppressed and flooding may occur through mechanism B. Hence, the flooding velocities would not be strong functions of the (hydraulic) diameter, and this is reflected in the correlations. It may also be noted that the data of Wallis & Makkenchery (1974) for the occurrence of a hanging film also show a diameter dependence for small diameter tubes but not for large diameter tubes.

The evidence presented so far is heuristic and in order to obtain a more concrete basis for the scenario, a study has been undertaken to estimate the form drag on a standing wave under typical flooding conditions. The flow field of a gas phase flowing over a standing wave located inside a channel has been calculated using computational fluid dynamics (CFD) techniques and has been shown to be a strong function of the channel dimensions. The results are then applied to calculate the gas velocity required to lift a standing wave under typical flooding conditions and it is shown that a transition in the flooding mechanism may be expected as the tube diameter increases.

2. PROBLEM FORMULATION AND SOLUTION METHODOLOGY

It is intended to show that the force exerted on an interfacial wave near the flooding point depends strongly on the tube diameter and that the tube diameter is an important factor in determining whether or not a wave can be transported up by the gas phase thereby influencing whether or not flooding can occur by mechanism A. In order to demonstrate this, it is necessary to obtain an accurate estimate of the drag force acting on the wave. In the present study the CFDS-FLOW3D computer code (CFDS 1993) has been used for this purpose. The formulation of the problem is as follows. A series of calculations has been made to determine the drag on a standing wave located on one of the walls of a rectangular channel of different heights. This case would correspond approximately to the drag acting on a circumferentially-coherent wave inside a tube because all the gas is forced to go over the wave. The resulting form drag coefficient is then correlated as a function of the reduction in cross-sectional area available for gas flow at the wave crest. Using this correlation, it is shown that the force on a wave decreases as the diameter increases and that it eventually exceeds the gas velocity required to suspend droplets, thereby inducing a change in the flooding mechanism. Details of these calculations are described below.

2.1. Flow domain and boundary conditions

The flow domain considered in the present study is shown schematically in figure 2(a). It consists of an inlet (AB) and an outlet (CD), a wall (AD) and a symmetry plane (BC) representing the central plane of the channel. A single wave is located on the wall; its dimensions are the same as

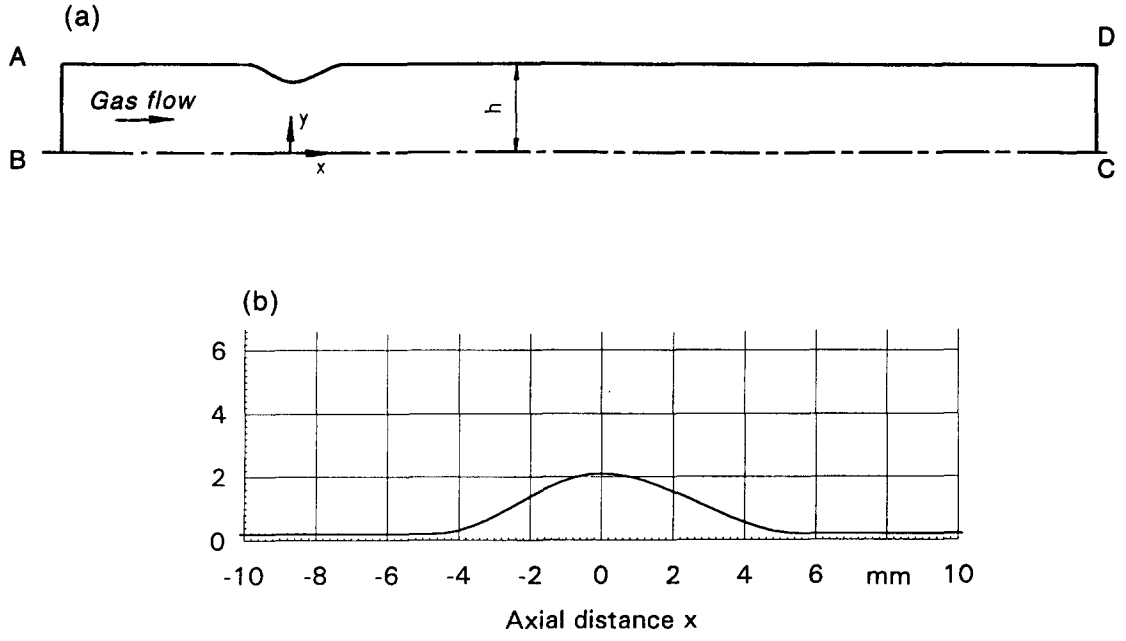

Figure 2. Formulation of the problem: (a) flow domain and boundary conditions and (b) detail of the standing wave.

those of the standing wave obtained experimentally by Shearer & Davidson (1965) for air–water countercurrent flow. As shown in figure 2(b), the wave is nearly symmetric and has an amplitude of 1.889 mm and a wavelength of about 8 mm.

The boundary conditions are as follows. Since the inlet and the outlet are well away from the wave [figure 2(a)], the flow is assumed to be fully-developed at either end. A no-slip boundary condition is specified, the wave being a stationary (standing) wave. (It must be noted that even for a standing wave, the interface may have a non-zero velocity; this effect is not taken into account in the present calculations, which however are thought to be valid as long as the (turbulent) gas flow velocity is much higher than the interface/wave velocity.) A symmetry boundary condition is specified along the centreline of the channel; this implies that a wave is present on the lower wall also. This, coupled with the fact that the flow is taken to be two-dimensional, means that these calculations correspond to the case of a coherent wave around the perimeter. The mass flow through the inlet and the outlet is varied so as to give different Reynolds numbers.

2.2. Governing equations and turbulence models

The incompressible, isothermal, steady fluid flow through the domain shown in figure 2 can be described mathematically in terms of a set of partial differential equations representing the conservation of mass and momentum and a set of boundary conditions. For turbulent flow, these equations are supplemented with a turbulence closure model. A number of turbulence models are available in the literature (see Rodi 1984 for a review). As part of the present investigation, an evaluaation of three of these turbulence models, namely, the standard k–ϵ model, the Reynolds stress model and the low Reynolds k–ϵ model, has been carried out. Of these, the first is the most widely used model for turbulent flows while the second is a more advanced model which can implicitly take account of effects such as streamline curvature which may be significant in flow over waves. The third has the advantage that, unlike the other two which use wall functions, it can be used to calculate the flow field right up to the wall. Details of the first two models as used in the CFDS-FLOW3D computer code have been described elsewhere (see Jayanti *et al.* 1990 for example) and are not discussed here. In the low Reynolds k–ϵ model, proposed initially by Jones & Launder (1972), two of the empirical constants used in the original k–ϵ model are modified in the near-wall region (where viscous effects may be important) by expressing them as functions of the turbulence Reynolds number defined as $\mathrm{Re}_t = \rho k^2/\mu\epsilon$ where k is the turbulent kinetic energy

and ϵ is the turbulent energy dissipation rate. This allows positional variations of these constants taking account, for example, of damping of turbulence very close to the wall and is therefore more realistic. The relevant functions and equations (Launder & Sharma 1974) are as follows. The Reynolds (turbulent) stresses obtained as a result of time-averaging the momentum conservation equation, is expressed in the form of a turbulent (eddy) viscosity which itself is a function of k and ϵ:

$$\mu_t = \rho \nu_t = \rho c_\mu' \frac{k^2}{\epsilon} \qquad [3]$$

where

$$c_\mu' = c_\mu \exp\left(-3.4 \Big/ \left(1 + \frac{\mathrm{Re}_t}{50}\right)^2\right) \qquad [4]$$

and

$$c_2' = c_2[1 - 0.3 \exp(-\mathrm{Re}_t^2)]. \qquad [5]$$

Here, c_μ and c_2 are constants in the original k–ϵ model (having values of 0.09 and 1.92, respectively) which are made functions of Re_t in the low Reynolds number k–ϵ model. Two extra terms, one each in the k-equation and the ϵ-equation, are added to account for the variation of the kinetic energy and the dissipation rate in the viscous sublayer. The final equations for k and ϵ are given below.Transport equation for k at low Reynolds number:

$$\frac{\partial k}{\partial t} + \frac{\partial (U_j k)}{\partial x_j} = \nu_t \left(\frac{\partial U_i}{\partial x_j} + \frac{\partial U_j}{\partial x_i}\right) \frac{\partial U_i}{\partial x_j} + \frac{\partial}{\partial x_j}\left[\left(\nu + \frac{\nu_t}{\sigma_k}\right)\frac{\partial k}{\partial x_j}\right] - \epsilon - 2\nu\left(\frac{\partial k^{1/2}}{\partial x_j}\frac{\partial k^{1/2}}{\partial x_j}\right). \qquad [6]$$

Transport equation for ϵ at low Reynolds number:

$$\frac{\partial \epsilon}{\partial t} + \frac{\partial (U_j \epsilon)}{\partial x_j} = c_1 \frac{\epsilon}{k} \nu_t \left(\frac{\partial U_i}{\partial x_j} + \frac{\partial U_j}{\partial x_i}\right) \frac{\partial U_i}{\partial x_j} + \frac{\partial}{\partial x_j}\left[\left(\nu + \frac{\nu_t}{\sigma_\epsilon}\right)\frac{\partial \epsilon}{\partial x_j}\right] - c_2' \frac{\epsilon^2}{k} + 2\nu\nu_t \left[\frac{\partial^2 U_i}{\partial x_j \partial x_j}\right]^2. \qquad [7]$$

The prediction of the static pressure distribution and the shear stress distribution for the case of flow over a stationary roll wave investigated experimentally by Miya (1970) by the three turbulence models are compared in figure 3. It is seen that while the pressure distribution has been predicted satisfactorily by all the three models, only the low Reynolds number model has been able to predict the steep fall in the wall shear stress just downstream of the wave crest. Similar results were obtained for other low Reynolds number flows leading to the general conclusion that it is possible to obtain a fairly accurate description of the pressure and the shear stress distribution when gas flows over large waves if an appropriate turbulence model, in this case, the low Reynolds number k–ϵ model, is used. In view of this, this model is used in all the cases investigated here. Note that the Reynolds number of the flow (see table 1) is also fairly small, and this may indicate that the standard high-Reynolds number models may not give good results.

2.3. Numerical solution procedure

A typical grid used in the calculations is shown in figure 4. The profile of the wave was based on that observed by Shearer & Davidson (1965). Some further grid points were added on either side of the wave in the axial (x-) direction so that the grid continued for about three wavelengths before and seven wavelengths after the wave. The wave itself was represented by 27 equally-spaced nodes and the nodes on either side of the wave were non-uniformly spaced and had an expansion factor of 1.4. A total of 46 cells were provided in the x-direction. The grid in the y-direction was non-uniformly spaced so as to ensure a high cell density near the wall. Depending on the size of the flow domain, a uniform expansion factor of 1.05 or 1.09 was used. The total number of cells in the y-direction was 50 in all cases. Thus, a total of 2300 points were used to represent the flow domain. In order to verify that the flow field near the wall was resolved sufficiently well, the flow

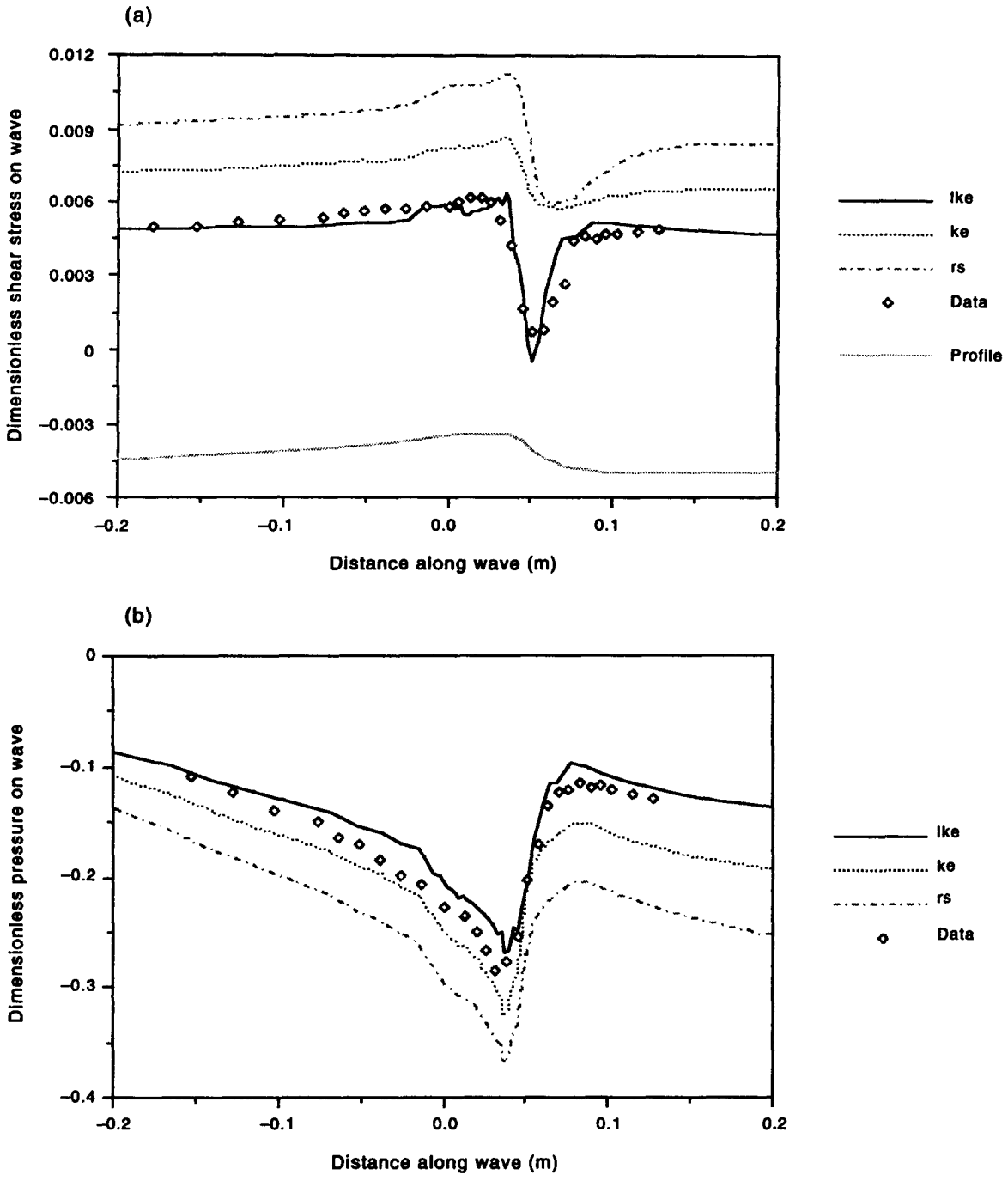

Figure 3. Variation of (a) non-dimensionalized static pressure and (b) non-dimensionalized shear stress induced by gas flowing over a roll wave. The squares are the data of Miya (1970) and the predictions of the standard k–ϵ model (ke), the Reynolds stress model (rs) and the low Reynolds number k–ϵ model (lke) are shown. The flow Reynolds number is 23,400.

field in a plane channel was calculated. It was found that the results agreed well with the universal velocity profile in the viscous sublayer and in the logarithmic overlap layer (White 1974) showing that the grid chosen was fine enough in the near-wall region.

The calculations were performed using the release 3.1 version of the CFDS-FLOW3D computer program (Jones *et al.* 1985; CFDS 1993). CFDS-FLOW3D uses a finite difference method on a general non-orthogonal body-fitted grid and has a polyalgorithmic structure whereby options are

Table 1. Details of the flow conditions investigated

Case	Domain height h (mm)	Channel height $2h$ (mm)	Gas velocity U (m/s)	Reynolds number $\mathrm{Re} = 4Uh/\nu$
12-6	12.7	25.4	6.3	17,780
25-6	25.4	50.8	6.3	35,560
38-6	38.1	76.2	6.3	53,340
12-4	12.7	25.4	4.0	11,288
12-9	12.7	25.4	9.3	26,246
9-9	9.5	19	9.3	19,634

available for the user to select from different discretisation schemes, linear equation solvers and physical models. It is based on a non-staggered method and uses an extended Rhie–Chow algorithm (Rhie & Chow 1983) to eliminate the chequerboard oscillations normally associated with the use of non-staggered grids. Details of the code and the turbulence models can be obtained from Burns & Wilkes (1987), Clarke & Wilkes (1989) and CFDS (1993).

The iterative calculations of the flow field proved difficult to converge with the low Reynolds number k–ϵ model and very small under relaxation factors had to be chosen. For this reason, the calculations were started with an under relaxation factor of 0.1 for the velocity components, and the default value of 0.65 was used after the first 500 iterations. This made the calculation time relatively short.

3. RESULTS

Calculations have been perfomed to determine the form drag over the wave as a function of the gas velocity and the tube diameter. Three gas velocities namely, 4.0, 6.3 and 9.3 m/s, were chosen

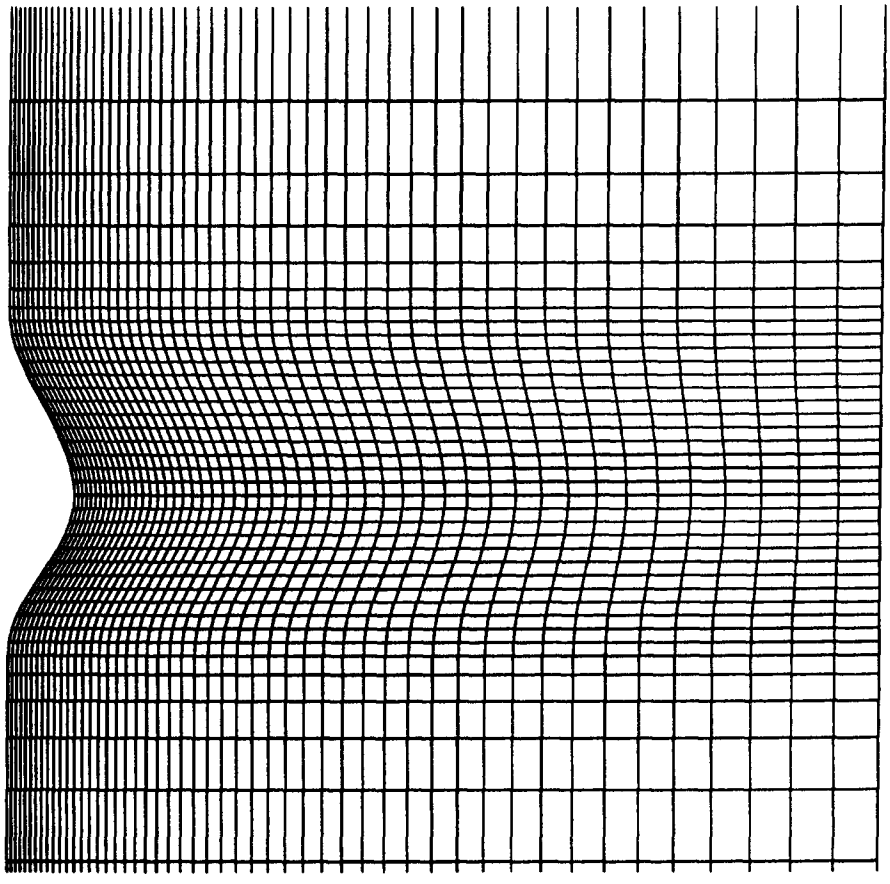

Figure 4. Typical grid used in the calculations with a uniform expansion factor in a y-direction of 1.05.

to cover the range of gas velocities under typical flooding conditions. To investigate the effect of the tube diameter, four channel heights were selected to cover the range of tube diameters normally used in experiments. The flow parameters in the calculations are summarized in table 1.

3.1. Typical flow field

A typical flow field obtained in the calculations is shown in figure 5 in the form of a vector plot of the velocities for case 12-6 (see table 1). For the sake of clarity, the profiles are shown at only selected axial locations. It can be seen that the flow is severely distorted in the region near the wave. As can be expected, the flow accelerates on the windward side of the wave and the velocity profile becomes very flat near the crest of the wave indicating the considerable thinning of the boundary layer due to the acceleration. The flow separates immediately after the crest of the wave and reattaches to the wall at about one wavelength further downstream. These effects can be seen much

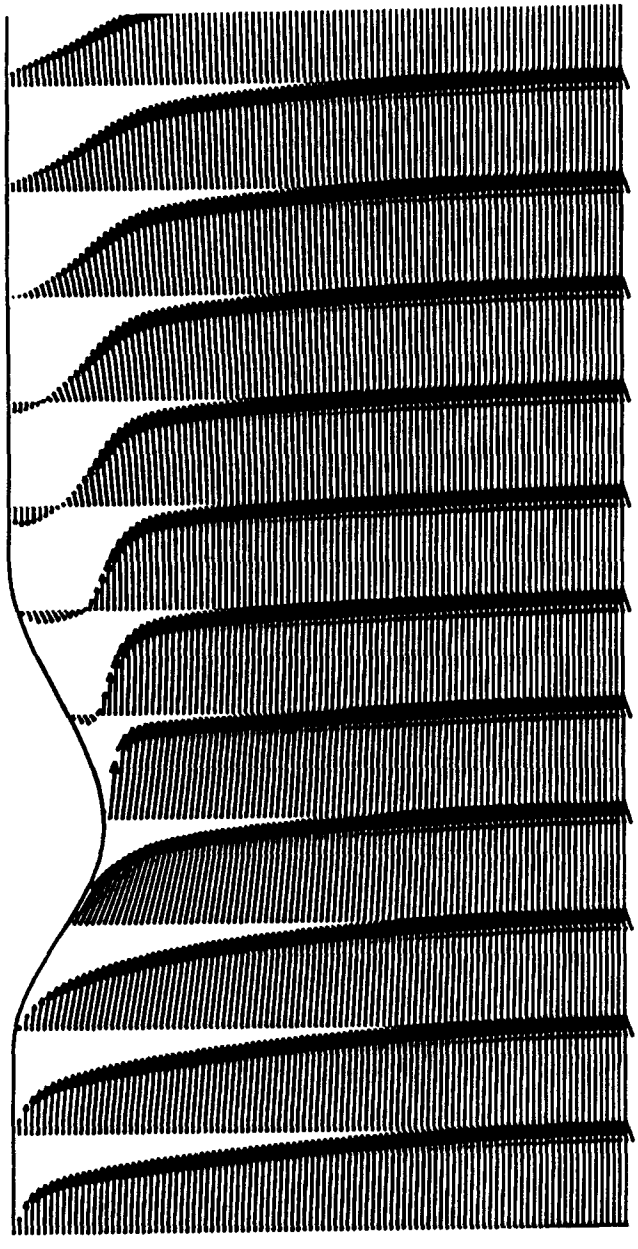

Figure 5. Velocity vectors obtained for the case of 12-6 (see table 1).

better in figure 6 where the axial velocity profiles just upstream and downstream of the wave are shown both in terms of actual velocity and in velocity non-dimensionalised by dividing by mean velocity. It is seen that in the latter, the velocity is negative in the region close to the wall and increases sharply to a value greater than the free stream value upstream of the wave. It is thus very different from the universal velocity profile which prevails upstream of the wave.

The variation of the pressure at the centre of the channel as well as on the wavy wall is shown in figure 7. The pressure along the centreline (symmetry plane) does not reach a minimum at the crest of the wave but at a point further downstream. This is similar to the phenomenon of a vena contracta occurring in flow through constrictions such as nozzles and orifices. There is a recovery of pressure further downstream but there is a net loss over the wave. The pressure on the wave surface shows a distinctly different variation. It increases on approach to the wave (similar to the increase upstream of a bluff body), then rapidly decreases up to the wave crest where it begins to recover. However, the flow then separates and the pressure remains nearly constant until the flow reattaches after which it recovers rapidly to its steady value.

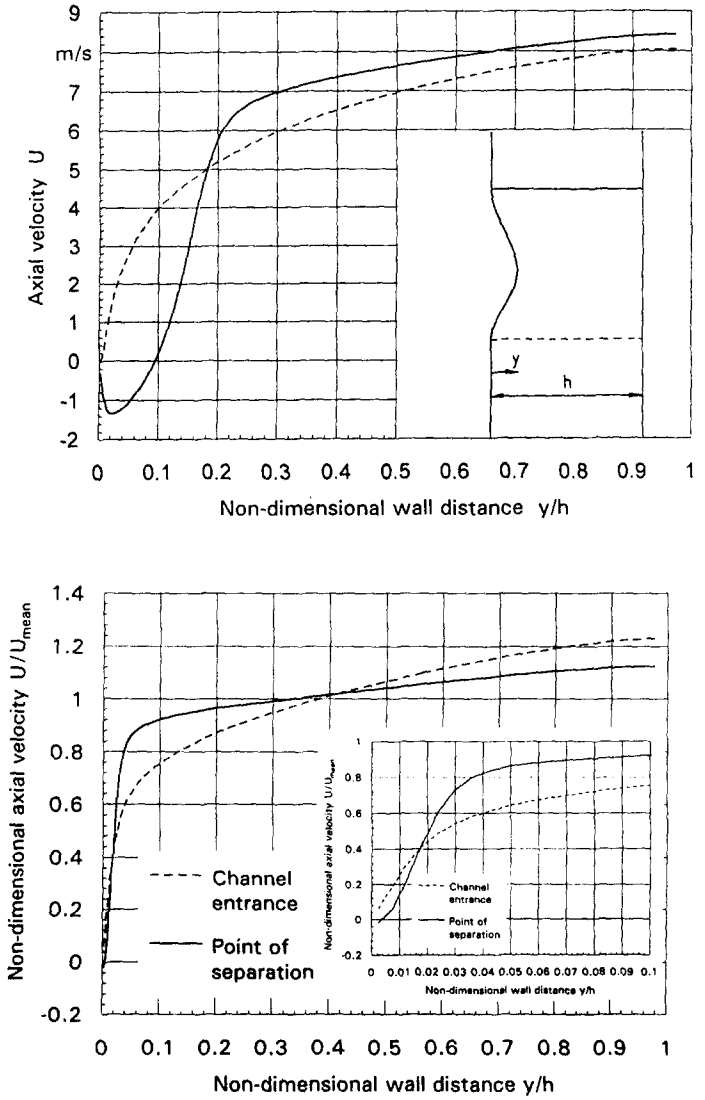

Figure 6. Velocity profiles just upstream and downstream of the wave for case 12-6.

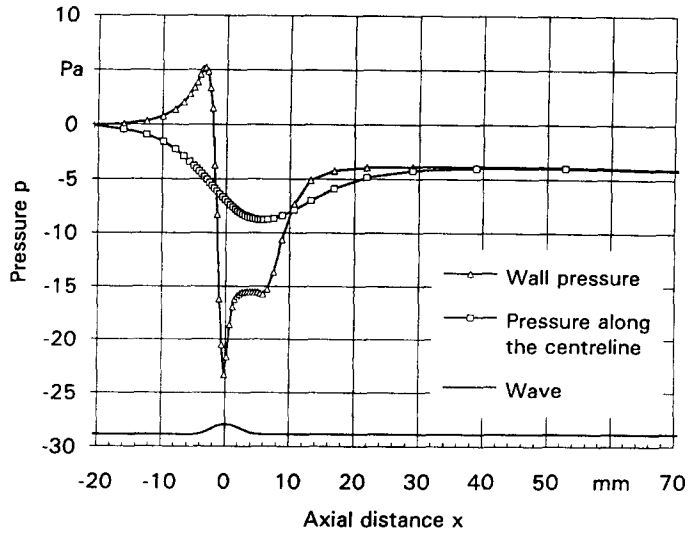

Figure 7. Variation of static pressure in the channel for the case of 12-6.

The variation of the shear stress on the wall is shown in figure 8. The absolute value of the wall shear stress (note that it is negative away from the wave) decreases as the wave is approached due to the adverse pressure gradient so that it is almost zero upstream of the wave. Due to the acceleration on the windward side of the wave, the wall shear stress decreases rapidly (increasing in magnitude) and reaches a minimum value just upstream of the crest. It then increases as rapidly, crosses zero (indicating flow separation) and remains positive for about one wavelength before decreasing back to its value in plane channel flow.

3.2. Variation with gas velocity and channel height

The results shown above are for the case of a channel height of $2h = 25.4$ mm and at a gas mean flow velocity of 6.3 m/s, and it is important to know how a variation in these parameters affects the results. The profile of the pressure on the channel wall is shown in figure 9 as a function of the channel height at a constant mean gas velocity of 6.3 m/s. It can be seen that there is a marked change in the pressure profile in two aspects. Firstly, the minimum in the pressure near the wave crest increases (in magnitude) as the channel height decreases. This is due to the fact the flow area

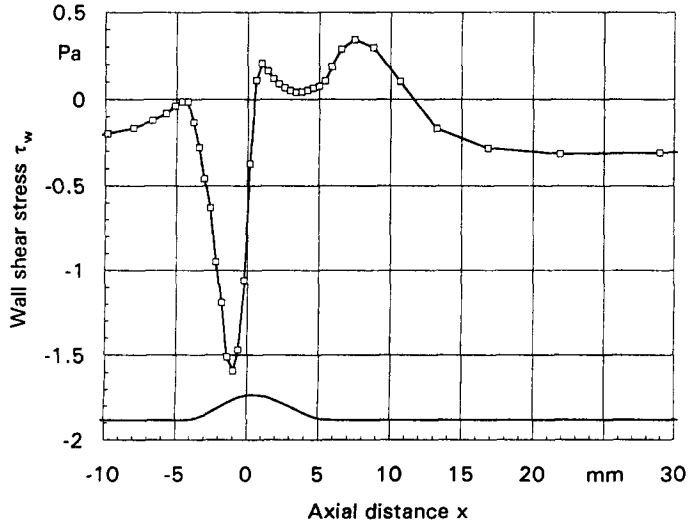

Figure 8. Variation of the wall shear stress for the case of 12-6.

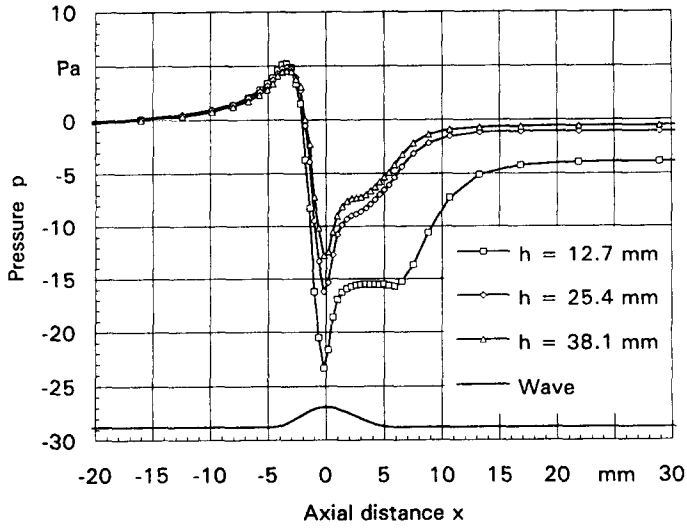

Figure 9. Effect of channel height on the wall pressure profile for a gas velocity of 6.3 m/s.

reduction at the crest is proportionally less in a larger channel than in a smaller channel for the same wave height. Secondly, although recirculation is present in all the cases, the extent of the recirculation, and the total pressure loss due to the constriction, vary significantly with the channel height.

The effect of the gas velocity is shown in figure 10 for a channel height of 25.4 mm. Here, the pressure is non-dimensionalized by dividing it by $\rho_G U_G^2$ where ρ_G is the gas density and U_G is the mean gas velocity upstream of the wave. It is interesting to note that the pressure variation remains nearly unchanged up to the point of separation after which it changes with the gas velocity. Both the point of separation and the point of reattachment appear to depend the gas velocity, and both are delayed as the velocity decreases. The variation, however, is not as remarkable as in the case of figure 9. These results are analogous to the case of flow through an orifice plate where the non-dimensional pressure loss is a strong function of the ratio of the orifice diameter to the tube diameter, but varies only weakly with the Reynolds number.

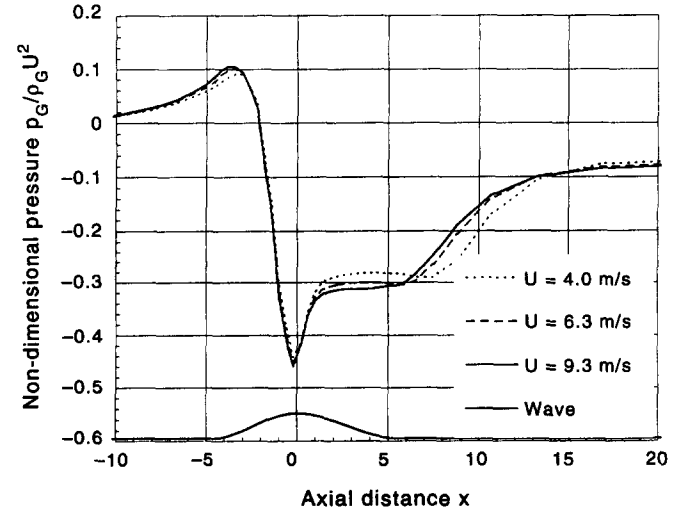

Figure 10. Effect of gas velocity on the pressure profile for a channel half-height of 12.7 mm.

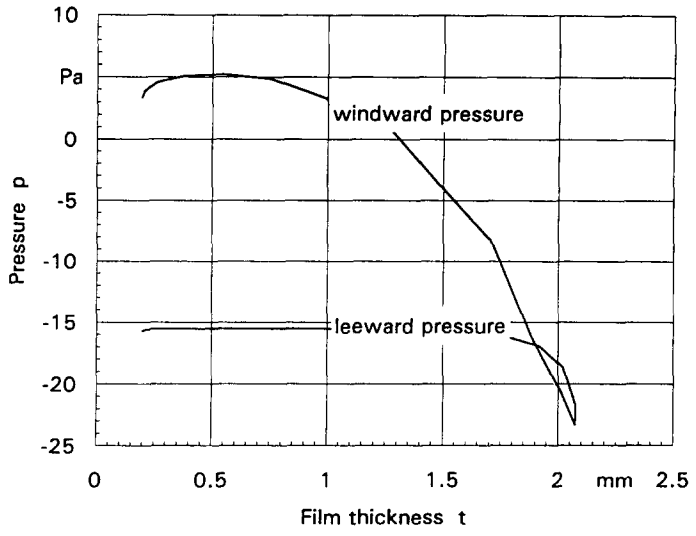

Figure 11. Pressure on the windward and the leeward sides of the wave for the case of 12-6.

3.3. Force on the wave

The force on the wave exerted by the gas phase consists of form drag due to the pressure variation and frictional force due to the action of the wall shear stress. A typical pressure variation on the windward and the leeward sides of the wave is shown in figure 11. It can be seen that the pressure on the leeward side is fairly constant due to flow separation and that it is significantly less than that on the windward side except in the region very close to the wave crest. Similarly, the wall shear stress on the windward side is also higher than that on the leeward side (figure 8). Integration of the pressure and the shear stress over the wave gives the form drag and the frictional force, respectively. These are listed in table 2 as a function of the channel height and the gas velocity. As expected for such a high-amplitude and short-wavelength wave, the form drag is the major contributor to F_G, the net force per unit perimeter exerted by the gas on the wave. Also, it can be seen that F_G increases as the channel height decreases at the same gas velocity. Since this is due to the reduction in the flow area at the wave crest, and since F_G is mainly due to form drag which correlates well with $\rho_G U_G^2$, the computational results can be correlated as

$$F_G = \rho_G U_G^2 (A - B\phi) \qquad [8]$$

where ϕ is the ratio of the flow area at the wave crest to that well upstream of the wave.

This correlation is plotted in figure 12 and shows good agreement with the numerical data. It can therefore be used to calculate the net force exerted by gas on waves typically encountered under flooding conditions.

4. APPLICATION TO FLOODING IN TUBES

The calculations described above are for two-dimensional flow in a rectangular channel of infinite width. Because the flow is two-dimensional, they represent a flow in which a two-dimensional wave,

Table 2. Summary of results from CFD calculations of forces on a standing wave

Channel height $2h$ (mm)	Gas velocity U (m/s)	Pressure force on wave (N/m)	Shear force on wave (N/m)	Total force (F_G) on wave (N/m)
19	9.3	0.0727	0.0183	0.0910
25.4	9.3	0.0597	0.0169	0.0766
25.4	6.3	0.0268	0.0083	0.0351
50.8	6.3	0.0173	0.0077	0.0250
76.2	6.3	0.0155	0.0069	0.0224

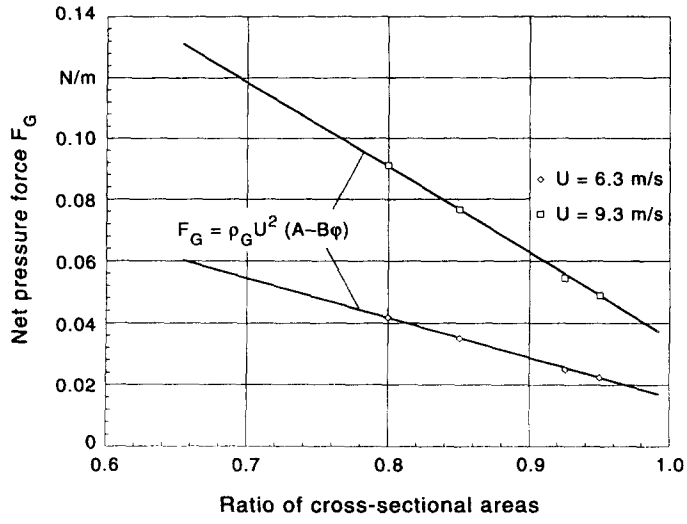

Figure 12. Correlation of the force on the wave as a function of the ratio of cross-sectional area.

i.e. one which spans the entire width of the channel, is present. In a cylindrical coordinate system, this is equivalent to a circumferentially coherent wave. The correlation for the gas force on the wave can now be used to estimate the gas velocity required for flooding assuming that the onset of flooding corresponds to the velocity at which the F_G is balanced by the weight per unit perimeter of the wave. This is done as follows.

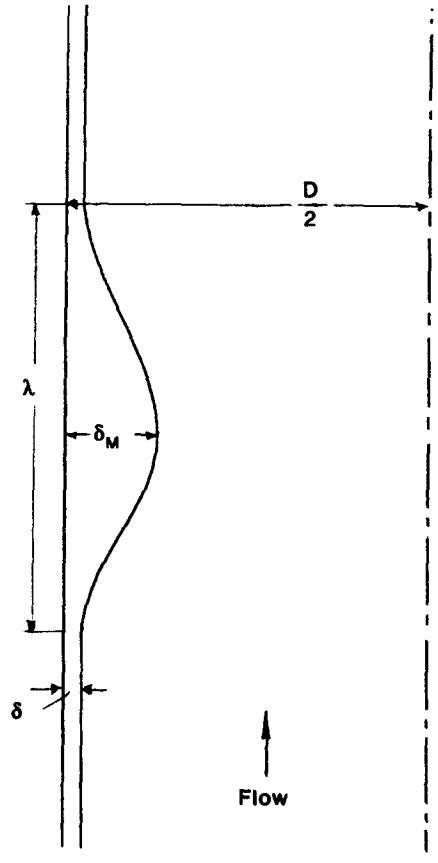

Figure 13. Application to flooding: estimation of the force on the wave and the weight of the wave.

With reference to figure 13, if δ_s is the substrate film thickness, δ_M the maximum film thickness (so that the waveheight is δ_M-δ_s) and λ the wavelength, then assuming the wave profile to be a sine function, the weight of the wave per unit perimeter is given by

$$F_w = 2\rho_L g\lambda(\delta_M - \delta_s)/\pi \quad [9]$$

For this wave, ϕ in equation [3] is given by

$$\phi_w = \frac{(D - 2\delta_M)^2}{(D - 2\delta_s)^2}. \quad [10]$$

The critical gas velocity at which the gas force equals the weight of the wave is then given by

$$U_{G,cr} = \sqrt{\frac{F_w}{\rho_G(A - B\phi_w)}}. \quad [11]$$

Thus, $U_{G,cr}$ is a function of the wave parameters. There is no precise knowledge of these parameters in a circular tube, especially because the wave characteristics will change significantly near flooding conditions (Zabaras & Dukler 1988; Biage *et al.* 1989). However, some idea of these can obtained from the data of Zabaras & Dukler who measured the film thickness as a function of time at various gas flow rates from zero to and beyond the flooding point. Their measurements were carried out for a tube diameter of 50.8 mm and for a liquid film Reynolds number (defined as $Re_{Lf} = 4U_{Lf}\delta/\nu_L$, where U_{Lf} is the liquid film velocity, δ is the mean film thickness and ν_L is the kinematic visocity of the liquid) ranging between 310 and 3100. For these experimental conditions, their results indicate that close to flooding, the mean film thickness is roughly 50% higher than that obtained from Nusselt's falling film analysis (Nusselt 1916):

$$\delta_N = \left(\frac{3\nu_L U_L D}{4g}\right)^{1/3}. \quad [12]$$

Since the substrate film thickness would be less than the mean film thickness, it is taken as $\delta_s = 0.8\delta = 1.2\delta_N$. The wave amplitude also increases close to the flooding point but is a function of the film flow rate. Their results show that ratio of the maximum film thickness, δ_M, to the mean film thickness, δ, decreases from 2.3 to 1.9 as Re_{Lf} is increased from 310 to 3100. Zabaras & Dukler did not measure the wavelength, λ, and a value of $\lambda = 6\delta_M$ has been chosen based on the results of Shearer & Davidson (1965).

With this selection of wave characteristics, it is now possible to calculate the flooding gas velocity (U_{Gc}) for a given liquid flow rate and a tube diameter. The calculated U_{Gc} is shown in table 3 as a function of the tube diameter and the liquid flow rate (in the form of $\sqrt{U^*_L}$). Also shown here are the predicted flooding velocities using the Wallis-type correlation (U_{GW}) of Hewitt & Wallis (1963) and the Kutetaldze-type correlation (U_{GK}) of Sun (1979). These correlations themselves were based on experimental data from different sources and they, rather than individual data points, may be expected to show better the trend with tube diameter.

Table 3. Gas velocity required for flooding according to various criteria

D (m)	$\sqrt{U^*_L}$	U_L (m/s)	δ (mm)	δ_M (mm)	U_{Gc} (m/s)	U_{Gw} (m/s)	U_{GK} (m/s)
0.025	0.15	0.011	0.42	0.96	5.8	7.6	11.0
0.050	0.15	0.016	0.59	1.30	8.5	10.8	10.3
0.075	0.15	0.019	0.72	1.51	10.2	13.2	9.8
0.10	0.15	0.022	0.83	1.66	11.3	15.2	9.5
0.025	0.20	0.020	0.50	1.14	6.6	6.6	9.8
0.050	0.20	0.028	0.71	1.50	9.5	9.3	8.9
0.075	0.20	0.034	0.87	1.70	11.1	11.4	8.3
0.10	0.20	0.040	1.01	1.85	12.8	13.2	7.9
0.025	0.25	0.031	0.58	1.29	7.3	5.7	8.6
0.050	0.25	0.044	0.83	1.65	10.1	8.0	7.6
0.075	0.25	0.054	1.01	1.85	11.7	9.8	7.0
0.10	0.25	0.062	1.17	2.09	13.5	11.3	6.5

It can be seen from the table that at a constant tube diameter, U_{Gc}, the gas velocity required for flooding induced by the transport of a coherent wave, is generally of the same order as U_{GW} for the three liquid flow rates considered. The calculations show a strong effect of the tube diameter and U_{Gc} increases significantly as the diameter increases. It is much less than U_{GK} for small diameters and much higher at larger diameters. Assuming that U_{GK} is a measure of the gas velocity required to suspend droplets (Taitel *et al.* 1980), it can be argued that for large tube diameters, the gas velocity required for entraining and carrying droplets upwards may become less than that required to transport the wave upwards. This means that as the tube diameter increases, mechanishm B is more likely to occur than mechanism A. It is interesting to note that Wallis & Makkenchery (1974) came to a similar conclusion on the occurrence of a hanging film around the flow reversal point in countercurrent flow. From their experiments, they noted that the critical gas velocity for the formation of a hanging film correlated with U_G^* for small diameter tubes and with Ku_G^* for large diameter tubes. They also observed that the wave structure on the hanging film was different in the two cases with a large coherent standing wave forming for small tube diameters (see figure 14). These results support the conclusions of the present study regarding the mechanism of flooding.

In the absence of a quantitative estimate of mechanism B, the point of transition of the flooding mechanism can only be determined experimentally. From the results in figure 1 and table 3, this transition can be put tentatively at a tube diameter of around 50 mm. Experiments, ideally with smooth inlet and outlet conditions, would therefore have to be conducted over a range of tube diameters of, say, 25–100 mm. These are being planned, and the results will be reported in due course.

The above model, in the present form, is unable to represent the relation between the liquid flow rate and the gas flow rate for a constant tube diameter. The reason for this is that the wave parameters are assumed in this model to be constant whereas in practice they would depend on the liquid flow rate in an, as yet, indeterminate way. Further calculations have shown that it is indeed possible to predict the correct trend with liquid flow rate by changing the wave parameters. The model can also explain the length effect on flooding. This effect would again be introduced through the wave properties, especially the shape and size, which would change with distance from the inlet and would therefore constitute different blockages at different lengths, thus experiencing different upward forces. Clearly, more data of wave properties near the flooding point are required to enable the model to predict the various parametric effects on flooding.

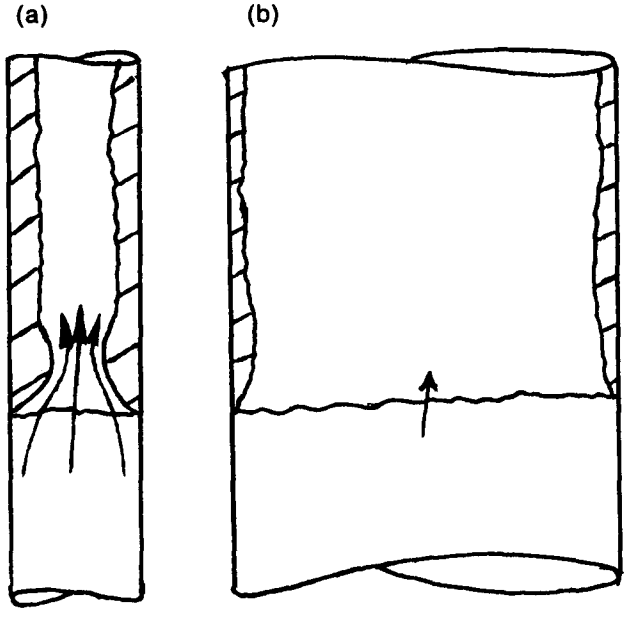

Figure 14. Shape of the hanging film reported by Wallis & Makkenchery (1974): (a) in small diameter tubes and (b) in large diameter tubes.

5. CONCLUSIONS

Calculations of the force exerted on a standing wave by gas flowing over it show that the drag is mainly due to the pressure variation around it and that it is a strong function of the channel dimensions. Extension of these results to typical flooding conditions in countercurrent flow in vertical tubes shows that the gas velocity required to transport waves upwards increases significantly as the tube diameter increases. It is argued therefore that for large diameter tubes, the gas velocity required to entrain and carry droplets upwards may be less than that required to transport a wave upwards so that flooding will occur by the former mechanism rather than the latter. The mechanism of flooding thus depends on the diameter of the tube; it is induced by upward transport of waves from near the bottom of the tube in small diameter tubes whereas it occurs due to entrainment and carryover of droplets near the liquid entry in large diameter tubes.

Acknowledgement—The authors gratefully acknowledge the financial support received from the Science and Engineering Research Council of the United Kingdom for this study.

REFERENCES

Bankoff, S. G. & Lee, S. C. 1986 A critical review of the flooding literature. In *Multiphase Science and Technology* (Edited by Hewitt, G. F., Delhaye, J. M. & Zuber, N.), Chap. 2. Hemisphere, New York.

Biage, M. 1989 Structure de la surface libre d'un film liquide ruisselant sur une plaque plane verticale et soumis à un contrecourant de gaz: transition vers l'écoulement cocourant ascendant. Ph.D. thesis, Institut National Polytechnique de Grenoble, Grenoble, France.

Biage, M., Delhaye, J. M. & Vernier, Ph. 1989 The flooding transition: a detailed experimental investigation of the liquid film before the flooding point. *ANS Proceedings, National Heat Transfer Conf.*, pp. 53–60.

Bradford, A. M. & Simpson, H. C. 1987 Penetration effects arising from simulated hot-leg injection in a 1/10 scale PWR test facility. *European Two-phase Flow Group Meeting*, Paper No. A4, Trondheim, Norway.

Burns, A. D. & Wilkes, N. S. 1987 A finite difference method for the computation of fluid flows in complex three-dimensional geometries. UKAEA Report No. AERE R12342.

CFDS 1993 *FLOW3D Release* 3.2.1: *User Manual*. Computational Fluid Dynamics Services (CFDS), Harwell Laboratory, AEA Technology, Didcot, England.

Clarke, D. S. & Wilkes, N. S. 1989 The calculation of turbulent flow in complex geometries using a differential stress model. UKAEA Report No. AERE R13428.

Clift, R., Pritchard, C. L. & Nedderman, R. M. 1966 The effect of viscosity on the flooding conditions in wetted wall columns. *Chem. Engng Sci.* **21**, 87–95.

Dukler, A. E. & Smith, L. 1979 Two-phase interaction in countercurrent flow: studies of the flooding mechanism. Annual Report, Nov. 1985–Oct. 1987, NUREG/CR-0617, U.S. Nuclear Regulatory Commission, Washington, DC.

Feind, F. 1960 Stromungensuntersuchungen bei Gegenstrom von Rieselfilmen und Gas in lotrechten Rohren. *VDI Forsch.* 481.

Govan, A. H. 1990 Modelling of vertical annular and dispersed two-phase flows. Ph.D. thesis, University of London, England.

Govan, A. H., Hewitt, G. F., Richter, H. J. & Scott, A. 1991 Flooding and churn flow in vertical pipes. *Int. J. Multiphase Flow* **17**, 27–44.

Hewitt, G. F. & Wallis, G. B. 1963 Flooding and associated phenomena in falling film flow in a vertical tube. UKAEA Report No. AERE R4022.

Hewitt, G. F., Lacey, P. M. C. & Nicholls, B. 1965 Transitions in film flow in a vertical tube. *Symp. on Two-phase Flow*, Paper B4, Exeter, England.

Imura, H., Kusuda, H. & Funatsu, S. 1977 Flooding velocity in a counter-current annular two-phase flow. *Chem. Engng Sci.* **32**, 79–87.

Jayanti, S., Wilkes, N. S., Clarke, D. S. & Hewitt, G. F. 1990 The prediction of flow over rough surfaces and its application to the interpretation of mechanisms of horizontal annular flow. *Proc. R. Soc. Lond.* **A431,** 71–88.

Jones, W. P. & Launder, B. E. 1972 The prediction of laminarisation with a two-equation model of turbulence. *Int. J. Heat Mass Transfer* **15,** 301–314.

Jones, I. P., Kightley, J. R., Thompson, C. P. & Wilkes, N. S. 1985 FLOW3D, a computer code for the prediction of laminar and turbulent flow and heat transfer: Release 1. UKAEA Report No. AERE R11825.

Kokkonen, I. & Tuimisto, H. 1990 Air/water countercurrent flow limitation experiments with full-scale fuel bundle structures. *Exp. Thermal Fluid Sci.* **3,** 581–587.

Launder, B. E. & Sharma, B. I. 1974 Application of the energy-dissipation model of turbulence to the calculation of flow near a spinning disc. *Lett. Heat Mass Trans.* **1,** 131–138.

McQuillan, K. W., Whalley, P. B. & Hewitt, G. F. 1985 Flooding in vertical two-phase flow. *Int. J. Multiphase Flow* **11,** 741–760.

Miya, M. 1970 Properties of roll waves. Ph.D. thesis, University of Illinois at Urbana-Champaign, IL.

Nusselt, W. 1916 Die oberflachenkondensation des Wasserdampfes. *VDI Zeitschr.* **60,** 541–546 and 569–575.

Rhie, C. M. & Chow, W. L. 1983 Numerical study of the turbulent flow past an air foil with trailing edge separation. *AIAA J.* **21,** 1527–1532.

Rodi, W. 1984 Turbulence models and their application in hydraulics—a state of the art review. In *Experimental and Mathematical Fluid Dynamics*, 2nd Edn. Presented by the IAHR Section on Fundamentals and Division II.

Shearer, C. J. & Davidson, J. F. 1965 The investigation of a standing wave due to gas blowing upwards over a liquid film; its relation to flooding in wall-wetted columns. *J. Fluid Mech.* **22,** 321–335.

Sun, K. J. 1979 Flooding correlations for BWR bundle upper tie plates and bottom side-entry orifices. In *Proc. of Multiphase Flow and Heat Transfer Symposium Workshop*, Miami Beach, FL (Edited by Veziroglu, T. N.), pp. 1615–1635.

Suzuki, S. & Ueda, T. 1977 Behaviour of liquid films and flooding in counter-current two-phase flow, Part 1: flow in circular tubes. *Int. J. Multiphase Flow* **3,** 517–532.

Taitel, Y., Barnea, D. & Dukler, A. E. 1980 Modelling flow pattern transitions for steady upward gas–liquid flow in vertical tubes. *AIChE J.* **26,** 345–354.

Wallis, G. B. 1961 Flooding velocities for air and water in vertical tubes. UKAEA Report No. AEEW R123.

Wallis, G. B. & Makkenchery, S. 1974 The hanging film phenomenon in vertical annular two phase flow. *J. Fluids Engng* **96,** 297–298.

White, F. M. 1974 *Viscous Fluid Flow*. McGraw–Hill, New York.

Zabaras, G. J. & Dukler, A. E. 1988 Counter-current gas–liquid annular flow including the flooding state. *AIChE J.* **34,** 389–396.